

Decoherence in electron transport: back-scattering, effect on interference and rectification

Abhiram Soori*

School of Physics, University of Hyderabad, C. R. Rao Road, Gachibowli, Hyderabad-500046, India

Udit Khanna

Department of Physics, Bar-Ilan University, Ramat Gan 52900, Israel

Decoherence is an undesirable, but ubiquitous phenomenon in quantum systems. Here, we study the effect of partial decoherence, induced via a Büttiker probe, on two-terminal electronic transport across one-dimensional quantum wires and rings, in both the linear and non-linear regimes. We find that dephasing causes backscattering when introduced locally in a ballistic channel. Further, we find that decoherence results in rectification when inversion is broken in the two-terminal transport setup by a combination of a local dephasing centre and a static impurity. Interestingly, the rectification strength and even its direction varies strongly with the relative distance between the probe and the scatterer. We further analyze how decoherence affects characteristic quantum effects in electronic transport, such as, Fabry-Pérot oscillations in double-barrier setups, and Aharonov-Bohm interference in one-dimensional rings, and find that the amplitude of oscillations in conductance is reduced by decoherence.

I. INTRODUCTION

Quantum effects appear in electronic transport through a number of remarkable phenomena, such as Fabry-Pérot oscillations and Aharonov-Bohm interference, that may be readily observed in appropriately designed mesoscopic devices. Beyond specific observations, perhaps the strongest manifestation of quantum dynamics is that transport through such devices can often be described (at least qualitatively) through a unitary scattering matrix relating the wavefunctions of incoming and outgoing modes [1]. This approach, pioneered by Landauer and Büttiker, relies on the electrons maintaining phase coherence while traversing through the device [2, 3]. However, phase information is inherently lost to some extent in any such device due to inelastic scattering, and it is important to understand the effects of this decoherence on quantum transport. Various quantitative effects of dephasing, such as the suppression of interference patterns, have been studied previously [4–7]. While rectification in two-terminal setup can be achieved by inelastic scattering when accompanied by broken time reversal symmetry [8,9], we show that rectification does not need breaking of time reversal symmetry. Instead, dephasing (by Büttiker probe method) can result in rectification when parity is broken.

The unitarity of the scattering matrix implies that the current in a two-terminal device should reverse its sign when the bias direction is reversed, i.e., the charge transport must be reciprocal in the absence of dephasing. Within the regime of linear response, this restriction is a special case of the Onsager-Casimir relations, which reflect the reversibility of the microscopic scattering processes [5, 8], and continue to hold even in the presence

of dephasing [9]. Beyond the linear regime, this symmetry constraint is *not necessarily respected* in the presence of inelastic scattering processes. It is interesting to understand the conditions under which such scattering may lead to a breakdown of reciprocity in nonlinear transport. Earlier works [10–14] considered this question in different setups that include a magnetic field, treating electron-electron interactions self-consistently and demonstrated that non-reciprocity may emerge if time-reversal symmetry is broken in interacting systems. In this work, we study a noninteracting model based on a quantum chain with local dephasing, and demonstrate that reciprocity may be violated even in the presence of time-reversal symmetry, by breaking inversion symmetry instead. Additionally, we study the effect of (partial) dephasing on Fabry-Pérot and Aharonov-Bohm interferences.

Microscopic modelling of the myriad interactions that may lead to phase-breaking is challenging even for small systems [15–17], and various phenomenological approaches have been developed to study such effects. These include adding imaginary terms to the Hamiltonian, or to the state [18, 19], as well as by modelling wavefunction collapse events [20]. Decoherence can also be introduced by time varying stochastic on-site potential [21]. In this work, we study the effects of decoherence on transport in the steady state through the Büttiker probe method [22], wherein a fictitious third terminal is connected to the device. This terminal is assumed to be in equilibrium at a carefully chosen voltage, such that there is no net transfer of charge from the probe to the setup. The probe does accept electrons from the setup at energies above the probe voltage, and then reinjects them into the device at a lower energy and with an arbitrary phase. The energy difference is absorbed within the probe. As such, the probe models the effects of inelastic scattering as well as the loss of phase information. The idea of introducing dephasing locally through an external

* abhirams@uohyd.ac.in

reservoir has been realized experimentally as well, in the context of a Mach-Zehnder interferometer [23]. From a different point of view, the probe may be considered as a measurement device that is continuously monitoring the average charge density at the site it is connected to. This is because the voltage on the probe is, in principle, an observable which depends on the local density distribution in the system [1].

Here, we consider the effect of decoherence on two-terminal steady state transport through several setups. Throughout this work, all reservoirs are treated as (spinless) one-dimensional chains (see Fig. 1). We begin, in section II, with transport across a single site (connected to the probe), and demonstrate that the inelastic scattering introduced by the probe not only introduces backscattering in an otherwise pristine quantum wire, but also leads to two parallel channels of transport, one of which is coherent while the other is incoherent. In section III, we consider transport across a cavity, modelled as a linear tight-binding chain, featuring Fabry-Pérot oscillations. We find that the probe acts as a selector, only affecting certain modes of the cavity and leaving the others intact. Then in section IV, we consider an Aharonov-Bohm ring, modelled as a 4-site tight-binding chain, and study how the dephasing introduced by the probe affects the interference pattern. Next, in section V, we consider a system with broken inversion symmetry, and show the emergence of rectification in presence of dephasing. Finally, we summarise and conclude in section VI.

II. BACKSCATTERING

A ballistic quantum wire connected to leads has a conductance of e^2/h in absence of impurities, which also means that the transmission probability is unity [1]. We introduce a Büttiker probe to the ballistic quantum wire connected to leads as shown in Fig. 1(a) and study the current-voltage characteristics in Fig. 1(b). We find that the conductance is less than e^2/h in presence of decoherence induced by the Büttiker probe, which implies that the decoherence induces backscattering in a ballistic channel.

The Hamiltonian to study this phenomenon is

$$H = -t \sum_{n=-\infty}^{\infty} (c_{n+1}^\dagger c_n + \text{h.c.}) - t \sum_{n=0}^{\infty} (d_{n+1}^\dagger d_n + \text{h.c.}) - t_P (c_0^\dagger d_0 + \text{h.c.}), \quad (1)$$

where c_n annihilates an electron on site- n in the ballistic quantum wire and d_n annihilates an electron at site n on the probe. Ballistic quantum wire extends from $n = -\infty$ to $n = \infty$, whereas the probe extends from $n = 0$ to $n = \infty$. The hopping strengths in the wire and the probe are t . The bond that connects the wire to the probe has a hopping strength t_P . We use the term “source”

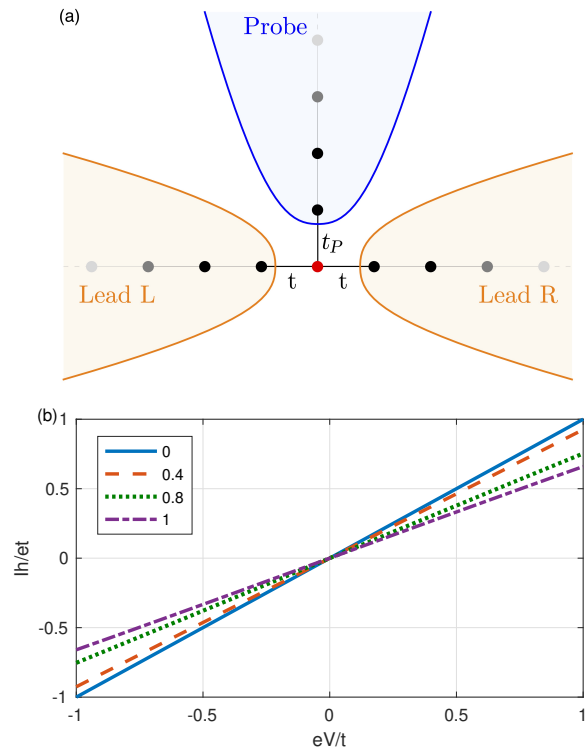


FIG. 1. Current-voltage characteristics of a ballistic quantum wire in presence of decoherence. (a) The setup comprises three reservoirs, modelled as one-dimensional chains with nearest neighbor hopping t , connected to a single site (marked in red). Leads L and R are connected to the site with hopping amplitude t , forming a ballistic quantum wire, and act as the source and drain for the current. While the voltage probe is connected with a hopping amplitude t_P and introduces decoherence at the site, without drawing any net current from the site. (b) I-V curves through the setup for different values of t_P/t . The decreasing slope of the I-V curves with increasing t_P/t is due to the backscattering introduced by the probe.

for the region $n \leq -1$ on the quantum wire, and the term “drain” for the region $n \geq 1$ on the quantum wire. Dispersion in the wire and the probe are $E = -2t \cos k$. The scattering wavefunction for an electron incident on the wire from the left with energy E has the form: $|\psi\rangle = \sum_{n=-\infty}^{\infty} \psi_{n,w} |n, w\rangle + \sum_{n=0}^{\infty} \psi_{n,p} |n, p\rangle$ (the subscript w/p refers to wire/probe), where

$$\begin{aligned} \psi_{n,w} &= e^{ikn} + r_k e^{-ikn}, \quad \text{for } n \leq -1, \\ &= t_k e^{ikn}, \quad \text{for } n \geq 1, \\ \psi_{n,p} &= t_{k,p} e^{ikn}, \quad \text{for } n \geq 0, \end{aligned} \quad (2)$$

where $k = \cos^{-1}(-E/2t)$. Under an applied bias V from source to drain, the currents in the source (I_{SS}), the

probe (I_{SP}) and the drain (I_{SD}) are given by

$$\begin{aligned} I_{SS} &= e \int_0^{eV} dE (1 - |r_k(E)|^2)/h, \\ I_{SP} &= e \int_0^{eV} dE |t_{k,p}(E)|^2/h, \\ I_{SD} &= e \int_0^{eV} dE |t_k(E)|^2/h. \end{aligned} \quad (3)$$

Now, a bias V_P is applied at the probe so that the current flows from the probe into source and drain in such way that the net current in the probe is zero. The currents due to the bias V_P on the probe into the source, drain and probe are I_{PS} , I_{PD} and $-I_{SP}$ respectively. These currents can be calculated in the following way. The wavefunction for an electron incident from the probe at energy E can be written as $|\psi\rangle = \sum_{n=-\infty}^{\infty} \psi_{n,w}|n,w\rangle + \sum_{n=0}^{\infty} \psi_{n,p}|n,p\rangle$, where

$$\begin{aligned} \psi_{n,p} &= e^{-ikn} + r_{k,p}e^{ikn} \quad \text{for } n \geq 0 \\ \psi_{n,w} &= t_{k,s}e^{-ikn} \quad \text{for } n \leq -1 \\ &= t_{k,d}e^{ikn} \quad \text{for } n \geq 1 \end{aligned} \quad (4)$$

Due to a voltage V_P applied in the probe terminal, the current in the probe (I_{PP}), the current in the source (I_{PS}), the current in the drain I_{PD} are given by:

$$\begin{aligned} I_{PP} &= e \int_0^{eV_P} dE (|r_{k,p}(E)|^2 - 1)/h, \\ I_{PS} &= -e \int_0^{eV_P} dE |t_{k,s}(E)|^2/h \\ I_{PD} &= e \int_0^{eV_P} dE |t_{k,d}(E)|^2/h \end{aligned} \quad (5)$$

The voltage of the probe V_P should be so chosen that $I_{PP} = -I_{SP}$. This choice of the probe voltage results in ‘‘voltage probe’’ [24]. The total current in the quantum wire under the influence of the two biases is $I_{SS} + I_{PS}$. The net current in the probe is zero. The phases of the backscattered currents in I_{SS} and I_{PS} will be different resulting in dephasing. In the limit $t_P \ll t$, I_{SP} becomes extremely small in magnitude, and the voltage V_P chosen so that the total current in the probe terminal is zero, can be regarded as the voltage measured at site $n = 0$ in the quantum wire. In Fig. 1(b), the numerically calculated current-voltage characteristics is plotted for different values of t_P . The I-V curve is found to be a straight line and the conductance decreases with increasing t_P .

Extent of dephasing

When a Buttiker probe is connected to a channel, a certain fraction of the incident current goes into the probe and an equal amount of current is supplied by the probe back into the channel. This fraction of current which is

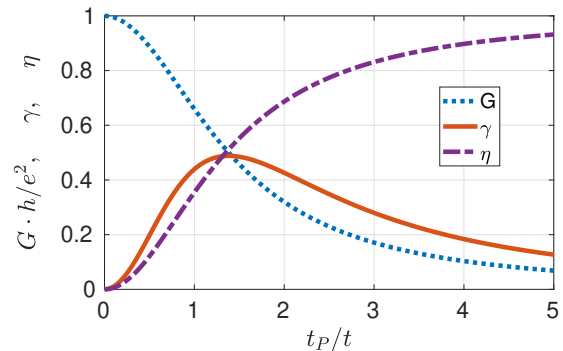


FIG. 2. Variation of the conductance (G), dephasing factor (γ) and coherent backscattering factor (η) with the strength of connection to the probe (t_P). Increasing t_P leads to higher backscattering and consequently to a monotonically decreasing G . When the coupling to the probe is weak, the dephasing (quantified by γ) increases with t_P . On the other hand, for large values of t_P/t a bound state localized at the junction appears in the spectrum, which leads to higher coherent backscattering but smaller dephasing. Consequently, the dephasing is nonmonotonic and maximal close to $t_P \approx t$. These results are for bias $V = t/e$.

injected back into the the channel is responsible for dephasing. We define the ratio of the current injected back from the probe to the current incident from the source as dephasing factor:

$$\gamma = \frac{(I_{PD} - I_{PS})h}{e^2V} \quad (6)$$

A part of the current injected back into the channel from the probe travels back into the source, which is purely incoherent. Also, there is a coherent backscattering that happens when electrons incident from the source scatter at the junction with the probe. We define coherent backscattering factor η as the ratio of the coherently backscattered current to the total backscattered current, which is given by the expression:

$$\eta = \frac{(e^2V/h - I_{SS})}{(e^2V/h - I_{SS} - I_{PS})} \quad (7)$$

The conductance, γ and η are plotted versus coupling to the probe t_P in Fig. 2. For large values of t_P , the two sites $n = 0$ on the wire and $n = 0$ on the probe form a dimer bound state and cause coherent backscattering. Thus, for large t_P , coherent backscattering is enhanced and dephasing is suppressed. Hence, the dephasing factor increases as t_P is increased from 0, reaches a maximum and then decreases. The conductance of the channel decreases monotonically with t_P , since the overall backscattering increases monotonically with t_P . At small t_P , both the coherent and the incoherent backscatterings contribute significantly, while at large t_P , the coherent backscattering dominates.

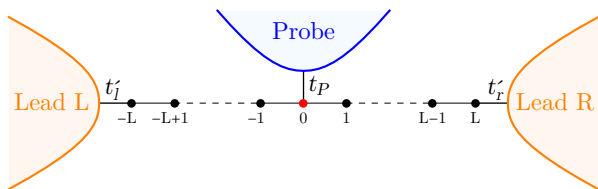


FIG. 3. Schematic of a Fabry-Pérot interferometer with de-cohering probe. The leads and the probe are modelled as 1D quantum wires (as depicted in Fig. 1), and connected to a 1D cavity of length $2L + 1$ with hopping amplitudes t'_l, t'_r and t_P , respectively. The probe is connected only to the central site of the cavity (marked in red) and hence, couples more strongly to the cavity modes with higher weight at this site. It is assumed that the chemical potential μ inside the cavity can be controlled through an external gate (not shown), which allows bringing different cavity modes within the bias window.

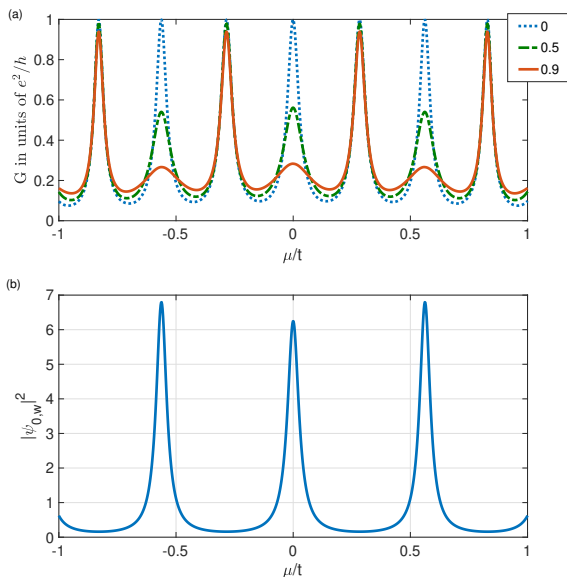


FIG. 4. (a) $G = I/V$ for a small bias V versus μ . Different curves are for different values of t_P/t shown in the legend. (b) $|\psi_{0,w}|^2$ for plane wave scattering in two-terminal device without the probe. The amplitude of oscillations decreases due to dephasing whenever $|\psi_{0,w}|^2$ is large. Parameters: $t'_l = t'_r = t'$, $t'/t = 0.4$, $V = 0.001t/e$, $L = 10$.

III. EFFECT ON FABRY-PÉROT INTERFERENCE

Let us consider a one dimensional channel of finite length weakly connected to leads on either sides. If the chemical potential in the channel can be tuned (which can be achieved by the application of a gate voltage), the conductance of the channel for a small bias should oscillate with a large amplitude when the chemical potential is changed [25–29]. This is the essence of Fabry-Pérot type interference. Now, if dephasing is introduced in the

channel at the centre, the amplitude of the Fabry-Pérot oscillations decreases. This can be seen in Fig. 4(a). The Hamiltonian for the study of this setup is,

$$\begin{aligned}
 H = & -t \sum_{n=-\infty}^{-L-1} (c_{n-1}^\dagger c_n + h.c.) - t'_l (c_{-L-1}^\dagger c_{-L} + h.c.) \\
 & -t \sum_{n=-L}^{L-1} (c_{n+1}^\dagger c_n + h.c.) - \mu \sum_{n=-L}^L c_n^\dagger c_n \\
 & -t'_r (c_{L+1}^\dagger c_L + h.c.) - t \sum_{n=L+1}^{\infty} (c_{n+1}^\dagger c_n + h.c.) \\
 & -t_P (c_0^\dagger d_1 + h.c.) - t \sum_{n=1}^{\infty} (d_{n+1}^\dagger d_n + h.c.) \quad (8)
 \end{aligned}$$

Here, μ is the chemical potential in the channel, which may be tuned through an external gate. The channel is connected to the source and drain leads through hopping matrix elements t'_l and t'_r which are assumed to be much smaller than the hopping t within the chain. This models a sharp tunnel barrier at either end of the cavity. The method of calculating the conductance when dephasing is present is same as that in the previous section.

When $t_P = 0$, the scattering wavefunction for an electron incident from left with zero energy has the form

$$\begin{aligned}
 \psi_{n,w} = & e^{ikn} + r_k e^{-ikn}, \quad \text{for } n < -L, \\
 = & s_+ e^{ik'n} + s_- e^{-ik'n}, \quad \text{for } -L \leq n \leq L, \\
 = & t_k e^{ikn}, \quad \text{for } n > L, \quad (9)
 \end{aligned}$$

where $k = \pi/2$, $k' = \cos^{-1}[-\mu/2t]$. In Fig. 4(b), $|\psi_{0,w}|^2$ is plotted versus μ . At finite t_P , the amplitude of Fabry-Pérot oscillations is suppressed largely at the values of μ for which $|\psi_{0,w}|^2$ is peaked (see, Fig. 4(a)). This is because, dephasing affects the Fabry-Pérot interference to a larger extent when the probability weight at the site of the dephasing is larger.

IV. EFFECT ON AHARONOV-BOHM OSCILLATIONS

To study the effect of dephasing on Aharonov-Bohm oscillations, we connect a four-site ring threaded by a flux to leads on either sides. One of the sites on the ring is connected to a Buttiker probe as shown in Fig. 5. The strength of hopping onto the probe determines the extent of dephasing. The Hamiltonian to study the effect of dephasing on Aharonov-Bohm oscillations is

$$\begin{aligned}
 H = & -t \sum_{n=-\infty}^{\infty} (c_{n+1}^\dagger c_n + h.c.) \\
 & -t (d_0^\dagger c_{-1} e^{i\phi} + d_0^\dagger c_1 + h.c.) - t_P (d_1^\dagger d_0 + h.c.) \\
 & -t \sum_{n=1}^{\infty} (d_{n+1}^\dagger d_n + h.c.) \quad (10)
 \end{aligned}$$

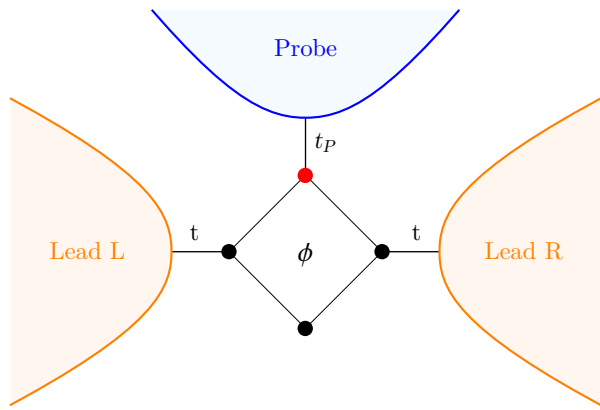


FIG. 5. Schematic of an Aharonov-Bohm interferometer with a decohering probe. The interferometer is modeled as a 4-site ring (with hopping amplitude t) threaded by flux ϕ . The source and drain leads are connected to two opposite sites of the ring with hopping amplitude t . The probe is connected to a third site (marked in red) with amplitude t_P . All reservoirs are modeled as 1D chains (as depicted in Fig. 1).

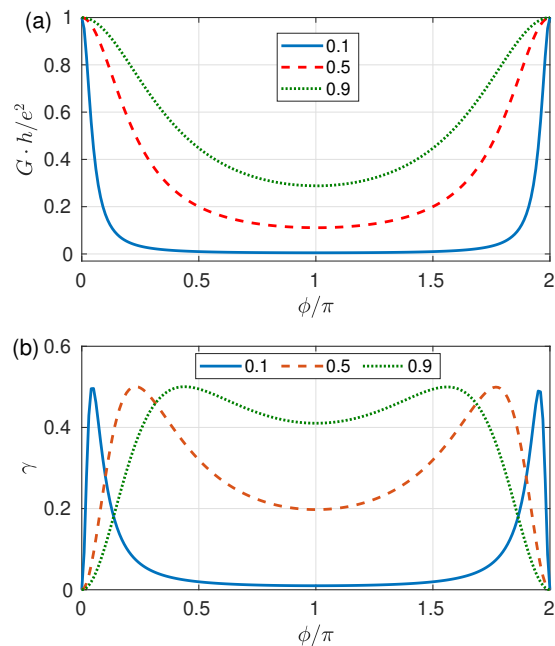


FIG. 6. (a) Conductance versus the flux through the ring ϕ for different values of t_P/t indicated in the legend. (b) Dephasing factor γ versus ϕ for different values of t_P/t indicated in the legend. Dephasing suppresses the amplitude of Aharonov-Bohm oscillations.

The current I in response to a bias V in this setup can be calculated using the same method as described in sec. II. The conductance $G = I/V$ for a small bias of $V = 0.001t/e$ is calculated as a function of the flux ϕ and plotted in Fig. 6(a). In absence of dephasing, the current across the ring is zero for $\phi = \pi$ due to destructive interference. On the other hand the current is large

for $\phi = 0$. Interestingly, at $\phi = \pi$, the current which is zero in purely coherent transport becomes nonzero as the dephasing (t_P) increases. This is in contrast to the case of ballistic channel, wherein dephasing suppresses conductance. The conductance of the ring oscillates as a function of the flux ϕ in the range $(0, 1)e^2/h$ for small values of t_P for which the dephasing is small. The amplitude of such oscillations decreases with increasing t_P for which the dephasing is larger. In Fig. 6(b), the extent of dephasing γ is plotted as a function of ϕ . The extent of dephasing is proportional to the current that flows through the probe when a bias is applied from source to drain. Such a current is zero for $\phi = 0$ due to interference effect and increases as ϕ increases. Therefore, the dephasing factor increases as ϕ increases from zero. But as ϕ increases beyond a certain value in the range $0 < \phi < \pi$, the current that flows from source to drain decreases. This makes the fraction of incident current that goes into the Büttiker probe decrease as ϕ increases beyond a certain value in the range $(0, \pi)$. This results in a peak in the graph of dephasing factor versus ϕ in the range $0 < \phi < \pi$.

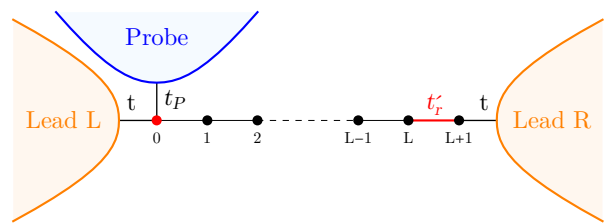


FIG. 7. Schematic of a quantum wire with a scatterer, which features rectification in presence of decoherence induced by a voltage probe. The scatterer is modelled as a disordered bond with hopping amplitude t'_r . The probe is connected to a site (marked in red) at a distance L from the scatterer with hopping amplitude t_P . All other hoppings are equal and denoted by t . The placement of the probe and the scatterer breaks the inversion symmetry of the setup and leads to finite rectification. All reservoirs are modelled as 1D chains (as depicted in Fig. 1).

V. DIODE EFFECT

Now, we study the possibility of diode effect in presence of dephasing. Breaking of parity is necessary for diode effect. We break parity by connecting site 0 to a Büttiker probe and making the hopping on the bond between sites L and $(L+1)$ weak. We take the Hamiltonian in eq. (8) and choose $t'_l = t$, $\mu = 0$. This setup is depicted in Fig. 7. The method of calculation of $I - V$ characteristics is same as the one explained in Sec. II. In Fig. 8, we plot $I - V$ characteristics for forward and reverse biases, diode effect coefficient Γ versus bias and the dephasing factor γ versus bias for $L = 3$ and $L = 10$. Here, we choose $t'_r = 0.2t$ and $t_P = t$. The hopping onto the

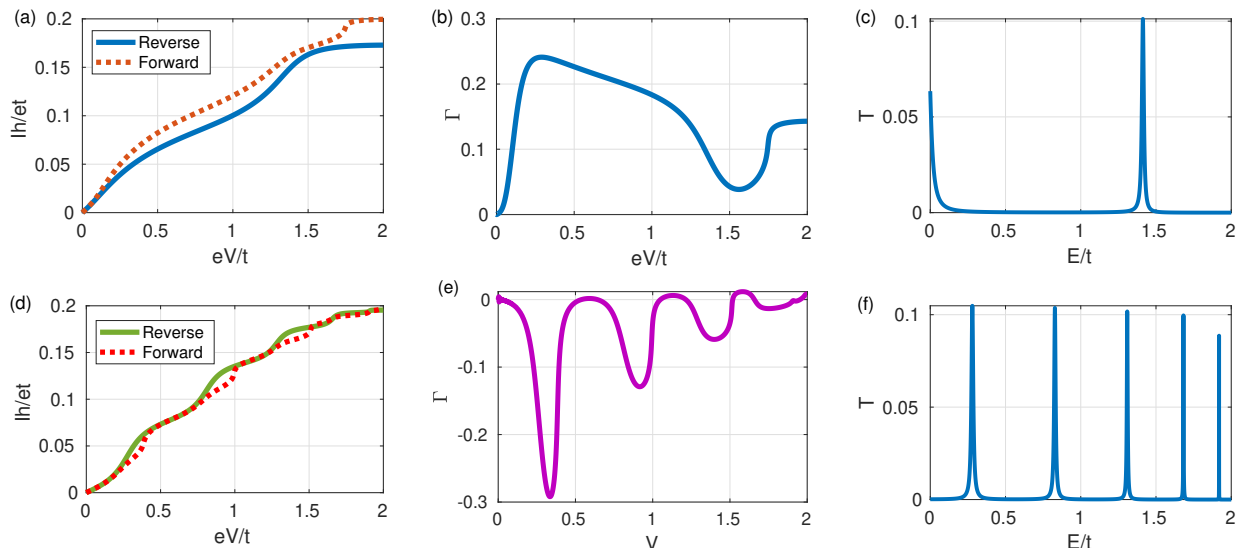


FIG. 8. Rectification induced by dephasing. (a,d) I-V characteristics of the setup with current flowing in different directions. Clearly, the current depends on the direction of the applied bias, indicating a rectification effect in the non-linear regime. (b,e) Diode effect coefficient $\Gamma = 2[I_F(V) - I_B(V)]/[I_F(V) + I_B(V)]$ as a function of bias V , for the forward (I_F) and backward (I_B) currents depicted in (a,d) respectively. The rectification effect is not monotonic as a function of the bias, due to the interplay of the dephasing with the interference going on inside the cavity. (c,f) Transmission probability of a coherent (but otherwise equivalent) cavity versus energy. The local minima in $\Gamma(V)$ observed in (b,e) are seemingly correlated with the resonances observed in (c,f). The length L was assumed to be 3 in (a,b,c) and 10 (d,e,f). The other parameters are identical for all figures, and taken to be $t'_r = 0.2t$, $t_P = t$, $\epsilon_0 = 30t$.

probe t_P is chosen to be t so that the dephasing is large, which is expected to result in a higher rectification. In the limit $t_P \ll t$, the diode effect coefficient becomes extremely small and there is no rectification. In principle, the choice $L = 0$ also breaks parity. But the I-V characteristics for this choice of L is linear and the diode effect does not show up. The diode effect coefficient Γ is defined by $\Gamma = 2[I_F(V) - I_B(V)]/[I_F(V) + I_B(V)]$. The diode effect coefficient shows oscillations as the bias is varied. $k(L+1) = n\pi$, where n is an integer, is the Fabry-Pérot interference condition. The values of the bias V at which this condition is satisfied is $V = -2t \cos[n\pi/(L+1)]$. For $L = 10$, these values of V are $0.28t, 0.83t, 1.3t, 1.7t, 1.9t$ for $n = 6, 7, 8, 9, 10$ respectively. At these values of the bias, the diode effect coefficient is large in magnitude as can be seen from Fig. 8(e).

To explain the features in Fig. 8(b,e), we consider a two terminal setup where, on an otherwise ballistic wire with hopping t , the bond between sites L and $L+1$ is made weak and also on site 0, an onsite energy ϵ_0 is introduced. There is no dephasing in this setup. Transmission probability for such a setup as a function of energy is shown in Fig. 8 (c) and Fig. 8 (f) for $t'_r = 0.2t$, $\epsilon_0 = 30t$. Current as a response to a bias is proportional to the integral of transmission probability over the bias window. Dephasing by voltage probe results in inelastic scattering where the electron that crosses the dephasing centre loses energy. So, for $L = 3$, when the bias V is small, the electrons at energy $E > 0$ incident from left to right first interact with the dephasing centre, lose energy and for

the lower energy electrons the transmission probability is higher (as compared to the case without dephasing) as can be seen from Fig. 8 (c). However, for the same bias window in the opposite direction, the electrons are incident from right to left. These electrons first interact with the resonant cavity, transmit to the left with a probability less than that for the forward bias and after the transmission, they interact with the dephasing centre. The electrons lose energy on dephasing and a fraction of the part that has undergone dephasing gets again backscattered to the right. So, on the whole, for a small bias, the current transmitted from left to right is higher than that from right to left resulting in positive diode effect coefficient that increases with bias. But as the bias is close to $1.4t/e$, the diode effect coefficient decreases and shows a valley. This is because, as the bias approaches a resonant energy from left, the electrons incident from left to right lose energy before transmission through the cavity resulting in lower transmitted current compared to the electrons incident from right to left which get transmitted through the cavity first (with a higher probability) and then interact with the dephasing centre, losing energy and getting trapped on the left side. A reasoning on similar lines explains the features of Fig. 8 (e).

VI. DISCUSSION

Suppression of amplitude of Fabry-Pérot oscillations due to dephasing studied in this work can be tested ex-

perimentally by coupling a resonant cavity to a probe and applying a gate voltage to the cavity. We could not find any work in the literature which studies the effect of dephasing on Fabry-Pérot oscillations by tuning the chemical potential. The effect of dephasing on Aharonov-Bohm interference is well-known [30, 31]. Our calculations qualitatively agree with these results, though the method followed differs in details. While diode effect in non-interacting four-terminal transport is not uncommon [32], two terminal quantum transport does not result in diode effect. We find that introducing dephasing in the transport channel results in diode effect in two terminal set-up when inversion symmetry is broken. This is in contrast to other works where time reversal symmetry breaking is needed to get diode effect in presence of dephasing [20, 33, 34]. Our finding that diode effect manifests in non-interacting systems in presence of dephasing when inversion is broken without the need of time-reversal breaking is a new finding. The idea of Büttiker probe to introduce dephasing in a channel in a controlled way has been experimentally realized [23]. In addition to a Büttiker probe, a barrier can be designed in experiments by an applied gate voltage to a small segment of a one-dimensional transport channel. Hence the set-ups proposed by us can be tested experimentally.

VII. SUMMARY AND CONCLUSION

In this work, we explore the impact of dephasing on electron transport in noninteracting systems using a Büttiker probe to introduce local dephasing. We observe that dephasing in a ballistic channel leads to backscattering. At low coupling to the Büttiker probe, both coherent and incoherent contributions to backscattering are present, while at high coupling strengths, coherent backscattering becomes dominant. The dephasing factor γ peaks at an intermediate coupling strength, whereas the coherent backscattering factor η increases monotonically with coupling.

In a cavity, local dephasing results in the suppression of Fabry-Pérot oscillations in conductance as the cavity's

chemical potential varies. This suppression is more pronounced when the wave function's probability weight is significant at the dephasing center. When the Büttiker probe is connected to an arm of an Aharonov-Bohm ring, dephasing can suppress backscattering, unlike in a ballistic channel where dephasing enhances backscattering. Additionally, dephasing reduces the amplitude of Aharonov-Bohm oscillations.

We also analyze the I-V characteristics of a one-dimensional channel with a dephasing center and a backscatterer (modeled by a weak hopping amplitude). We find that dephasing along with broken inversion results in rectification. This setup exhibits rectification, with the diode effect coefficient oscillating with bias. The coefficient can switch from positive to negative depending on the distance between the dephasing center and the backscatterer. We provide explanations for the peaks and valleys in the diode effect coefficient as a function of bias.

While rectification is impossible in coherent two-terminal noninteracting metallic systems due to the unitarity of the scattering matrix, it can occur in superconducting systems with coherent scattering when time reversal and inversion are broken [35]. Additionally, rectification is a known phenomenon in four-terminal noninteracting setups [32]. We show that dephasing by Büttiker probe can cause diode effect in inversion broken metallic transport channel. Since the probe acts a measurement device, our results also provide a glimpse of how the quantum dynamics of these systems are affected under (local) continuous monitoring of charge density [36, 37].

ACKNOWLEDGMENTS

AS thanks SERB Core Research grant (CRG/2022/004311) and University of Hyderabad Institute of Eminence PDF for funding. UK was supported by fellowships from the Israel Science Foundation (ISF, Grant No. 993/19), the US-Israel Binational Science Foundation (BSF Grant No. 2016130), and the NSF-BSF Grant No. 2018726.

-
- [1] S. Datta, *Electronic transport in mesoscopic systems* (Cambridge University Press, Cambridge, 1995).
 - [2] R. Landauer, "Spatial variation of currents and fields due to localized scatterers in metallic conduction," *IBM J. Res. Dev.* **1**, 223–231 (1957).
 - [3] M. Büttiker, "Absence of backscattering in the quantum Hall effect in multiprobe conductors," *Phys. Rev. B* **38**, 9375–9389 (1988).
 - [4] A. Stern, Y. Aharonov, and Y. Imry, "Phase uncertainty and loss of interference: A general picture," *Phys. Rev. A* **41**, 3436–3448 (1990).
 - [5] Y. Imry, *Introduction to Mesoscopic Physics* (Oxford University Press, Oxford, 2002).
 - [6] P. W. Brouwer and C. W. J. Beenakker, "Voltage-probe and imaginary-potential models for dephasing in a chaotic quantum dot," *Phys. Rev. B* **55**, 4695–4702 (1997).
 - [7] O. Entin-Wohlman and A. Aharony, "Three-terminal thermoelectric transport under broken time-reversal symmetry," *Phys. Rev. B* **85**, 085401 (2012).
 - [8] H. B. G. Casimir, "On onsager's principle of microscopic reversibility," *Rev. Mod. Phys.* **17**, 343–350 (1945).
 - [9] M Büttiker, "Four-terminal phase-coherent conductance," *Phys. Rev. Lett.* **57**, 1761 (1986).
 - [10] M Buttiker, "Capacitance, admittance, and rectification properties of small conductors," *J. Phys.: Condens. Mat-*

- ter **5**, 9361 (1993).
- [11] D. Sánchez and M. Büttiker, “Magnetic-field asymmetry of nonlinear mesoscopic transport,” *Phys. Rev. Lett.* **93**, 106802 (2004).
- [12] B. Spivak and A. Zyuzin, “Signature of the electron-electron interaction in the magnetic-field dependence of nonlinear $I-V$ characteristics in mesoscopic systems,” *Phys. Rev. Lett.* **93**, 226801 (2004).
- [13] A. R. Hernández and C. H. Lewenkopf, “Nonlinear conductance in a ballistic Aharonov-Bohm ring,” *Phys. Rev. Lett.* **103**, 166801 (2009).
- [14] J. S. Lim, D. Sánchez, and R. López, “Magnetoasymmetric transport in a mesoscopic interferometer: From the weak to the strong coupling regime,” *Phys. Rev. B* **81**, 155323 (2010).
- [15] M. Lotem, A. Weichselbaum, J. von Delft, and M. Goldstein, “Renormalized Lindblad driving: A numerically exact nonequilibrium quantum impurity solver,” *Phys. Rev. Res.* **2**, 043052 (2020).
- [16] T. Jin, M. Filippone, and T. Giamarchi, “Generic transport formula for a system driven by markovian reservoirs,” *Phys. Rev. B* **102**, 205131 (2020).
- [17] T. Jin, J. S. Ferreira, M. Filippone, and T. Giamarchi, “Exact description of quantum stochastic models as quantum resistors,” *Phys. Rev. Res.* **4**, 013109 (2022).
- [18] Y. Gefen, Y. Imry, and M. Ya. Azbel, “Quantum oscillations and the Aharonov-Bohm effect for parallel resistors,” *Phys. Rev. Lett.* **52**, 129–132 (1984).
- [19] K. B. Efetov, “Temperature effects in quantum dots in the regime of chaotic dynamics,” *Phys. Rev. Lett.* **74**, 2299–2302 (1995).
- [20] P. Bredol, H. Boschker, D. Braak, and J. Mannhart, “Decoherence effects break reciprocity in matter transport,” *Phys. Rev. B* **104**, 115413 (2021).
- [21] L. Mejía, U. Kleinekathöfer, and I. Franco, “Coherent and incoherent contributions to molecular electron transport,” *J. Chem. Phys.* **156**, 094302 (2022).
- [22] M. Büttiker, “Coherent and sequential tunneling in series barriers,” *IBM J. Res. Dev.* **32**, 63 (1988).
- [23] P. Roulleau, F. Portier, P. Roche, A. Cavanna, G. Faini, U. Gennser, and D. Mailly, “Tuning decoherence with a voltage probe,” *Phys. Rev. Lett.* **102**, 236802 (2009).
- [24] S. Bedkihal, M. Bandyopadhyay, and D. Segal, “The probe technique far from equilibrium: Magnetic field symmetries of nonlinear transport,” *Eur. Phys. J. B* **86**, 506 (2013).
- [25] A. Soori, S. Das, and S. Rao, “Magnetic-field-induced Fabry-Pérot resonances in helical edge states,” *Phys. Rev. B* **86**, 125312 (2012).
- [26] A. Soori and S. Mukerjee, “Enhancement of crossed Andreev reflection in a superconducting ladder connected to normal metal leads,” *Phys. Rev. B* **95**, 104517 (2017).
- [27] A. Soori, “Transconductance as a probe of nonlocality of Majorana fermions,” *J. Phys.: Condens. Matter* **31**, 505301 (2019).
- [28] A. Soori, “Finite transverse conductance and anisotropic magnetoconductance under an applied in-plane magnetic field in two-dimensional electron gases with strong spin-orbit coupling,” *J. Phys.: Condens. Matter* **33**, 335303 (2021).
- [29] A. Soori, “Tunable crossed Andreev reflection in a heterostructure consisting of ferromagnets, normal metal and superconductors,” *Solid State Commun.* **348-349**, 114721 (2022).
- [30] T. P. Pareek, Sandeep K. Joshi, and A. M. Jayannavar, “Comparison between two models of dephasing in mesoscopic systems,” *Phys. Rev. B* **57**, 8809–8811 (1998).
- [31] C. Benjamin and A. M. Jayannavar, “Dephasing via stochastic absorption: A case study in aharonov-bohm oscillations,” *Phys. Rev. B* **65**, 153309 (2002).
- [32] A. M. Song, A. Lorke, A. Kriele, J. P. Kotthaus, W. Wegscheider, and M. Bichler, “Nonlinear electron transport in an asymmetric microjunction: A ballistic rectifier,” *Phys. Rev. Lett.* **80**, 3831–3834 (1998).
- [33] M. Bandyopadhyay, S. Ghosh, A. Dubey, and S. Bedkihal, “Flux dependent current rectification in geometrically symmetric interconnected triple-dot aharonov-bohm interferometer,” *Physica E* **133**, 114786 (2021).
- [34] S. Bedkihal, M. Bandyopadhyay, and D. Segal, “Magnetic field symmetries of nonlinear transport with elastic and inelastic scattering,” *Phys. Rev. B* **88**, 155407 (2013).
- [35] A. Soori, “Josephson diode effect in junctions of superconductors with band asymmetric metals,” *J. Phys.: Condens. Matter* **36**, 335303 (2024).
- [36] R. Hussein, J. Gómez-García, and S. Kohler, “Monitoring quantum transport: Backaction and measurement correlations,” *Phys. Rev. B* **90**, 155424 (2014).
- [37] X. Turkeshi, L. Piroli, and M. Schirò, “Density and current statistics in boundary-driven monitored fermionic chains,” *Phys. Rev. B* **109**, 144306 (2024).